Polymer-Coated $NaYF_4:Yb^{3+}$, Er^{3+} Upconversion Nanoparticles for Charge-Dependent Cellular Imaging

Jiefu Jin,[‡] Yan-Juan Gu,[†] Cornelia Wing-Yin Man,[†] Jinping Cheng,[§] Zhenhua Xu,[‡] Yue Zhang,[‡] Huaishan Wang,[†] Vien Hoi-Yi Lee,[†] Shuk Han Cheng,[§] and Wing-Tak Wong[†,∥,*]

[†]Department of Applied Biology and Chemical Technology, The Hong Kong Polytechnic University, Hung Hom, Kowloon, Hong Kong, [‡]Department of Chemistry, The University of Hong Kong, Pokfulam Road, Hong Kong, [§]Department of Biology and Chemistry, City University of Hong Kong, Hong Kong, and [∥]PearL Materia Medica Development (Shenzhen) Ltd., Shenzhen 518057, China

ABSTRACT Lanthanide-doped upconversion nanoparticles (UCNPs) are considered promising novel near-infrared (NIR) bioimaging agents with the characteristics of high contrast and high penetration depth. However, the interactions between charged UCNPs and mammalian cells have not been thoroughly studied, and the corresponding intracellular uptake pathways remain unclear. Herein, our research work involved the use of a hydrothermal method to synthesize polyvinylpyrrolidone-coated UCNPs (UCNP-PVP), and then a ligand exchange reaction was performed on UCNP-PVP, with the help of polyethylenimine (PEI) and poly(acrylic acid) (PAA), to generate UCNP-PEI and UCNP-PAA. These polymer-coated UCNPs demonstrated good dispersibility in aqueous medium, had the same elemental composition and crystal phase, shared similar TEM and dynamic light scattering (DLS) size distribution, and exhibited similar upconversion luminescence efficiency. However, the positively charged UCNP-PEI evinced greatly enhanced cellular uptake in comparison with its neutral or negative counterparts, as shown by multiphoton confocal microscopy and inductively coupled plasma mass spectrometry (ICP-MS) measurements. Meanwhile, we found that cationic UCNP-PEI can be effectively internalized mainly through the clathrin endocytic mechanism, as revealed by colocalization, chemical, and genetic inhibitor studies. This study elucidates the role of the surface polymer coatings in governing UCNP–cell interactions, and it is the first report on the endocytic mechanism of positively charged lanthanide-doped UCNPs. Furthermore, this study provides important guidance for the development of UCNPs as specific intracellular nanoprobes, allowing us to control the UCNP–cell interactions by tuning surface properties.

KEYWORDS: upconversion nanoparticles · ligand exchange · charge-dependent cellular uptake · clathrin-mediated endocytosis

Live-cell fluorescence imaging has caught the attention of many researchers due to its high sensitivity and excellent selectivity in monitoring molecular localization, cellular processes, and gene expression in live cells.[1,2] Conventional fluorescence imaging involves the use of visible or ultraviolet (UV) light as the sensitization source. However, this sensitization mode has several disadvantages, such as interference from autofluorescence, strong absorption, and scattering of various biological molecules. Near-infrared (NIR) fluorescence imaging is an emerging imaging modality with high signal-to-noise ratio and deep tissue penetration.[3−5] However, commonly used NIR chromophores have certain drawbacks, such as poor photostability of organic dyes[6] and acute toxicity of semiconductor quantum dots.[7] This largely limits their versatility as biological fluorescence probes. Recently, lanthanide-doped upconversion nanoparticles (UCNPs), which absorb NIR long-wavelength excitations and convert to short-wavelength emissions, have been considered an important alternative to NIR organic fluorophores and quantum dots for bioimaging applications.[8,9] Lanthanide-doped UCNPs possess typical characteristics of lanthanide luminescence, including narrow emission spectra and long lifetimes. Moreover, UCNPs can be excited by using NIR light at a spectral range of 700−1000 nm, where the absorption coefficients of water, lipid, hemoglobin, and other biological components are minimal.[4] Among the host matrixes that can house lanthanide ions to initiate upconverting luminescence, $NaYF_4$ with Yb^{3+} and Er^{3+} dopants is known to be the most efficient NIR-to-visible upconverting materials,[10] where the excitation source can be chosen with low excitation intensity ($1-10^3$ $W \cdot cm^{-2}$), such as cheap and readily available continuous wave diode lasers.[11] Thereafter, a range of biocompatible and functional UCNPs have been developed for nucleotide detection,[12−15] cellular imaging,[16−22] *in vivo* imaging,[23−35] and drug/gene delivery.[36−38]

However, our knowledge of UCNP–cell interactions is limited, and their intracellular uptake pathways remain unexplored. The most common interaction, electrostatic interaction between the charged NPs and the negatively charged plasma membrane of cells, will largely affect the NPs in cytotoxicity, uptake efficiency, and cellular localization.[39−41] Previous studies[39,42] have shown that NPs were often internalized into

* Address correspondence to bcwtwong@polyu.edu.hk.

Received for review May 24, 2011 and accepted September 9, 2011.

Published online September 09, 2011
10.1021/nn201896m

the cells *via* a process termed pinocytosis, which is a type of endocytosis that involves at least four basic mechanisms: macropinocytosis (>1 μm), clathrin-mediated endocytosis (~120 nm), caveolae-mediated endocytosis (~60 nm), and clathrin- and caveolae-independent endocytosis. Surface coatings on UCNPs would play an important role in their cellular entry through the plasma membrane and the corresponding internalization pathways. Therefore, the investigations on the effects of surface coatings are crucial not only for the engineering of UCNPs for targeted cell labeling but also for controlled gene/drug delivery with high therapeutic capacity.

In our study, we designed and prepared a series of polymer-coated UCNPs based on a simple ligand exchange approach. Select surface-mounted polymers endowed the UCNPs with different surface charges (positive, neutral, and negative). We found that positively charged UCNPs have significantly enhanced cellular uptake in several human cell lines including cervical carcinoma (HeLa), glioblastoma (U87MG), and breast carcinoma (MCF-7) cells. We have also proved that these cationic UCNPs can be uptaken mainly *via* clathrin-coated vesicular endocytosis. Our work presents a picture of how the polymer coatings on the UCNP surface affect their ionic interactions with mammalian cells, and it is the first report on unraveling the cellular uptake pathway of positively charged lanthanide-doped UCNPs.

RESULTS AND DISCUSSION

Synthesis and Characterization. UCNP-PVP was synthesized using a hydrothermal reaction based on the procedures reported in the literature but with slight modification.[43] The commonly used polymer, PVP, serves as a structure regulating agent for chelating lanthanide ions to control the size, morphology, and shape of the obtained nanoparticles. These nanoparticles exhibit good dispersibility in aqueous medium (Figure 1a) and a relatively narrow size distribution (Figure 1b) with an average diameter of 50 nm. This result was obtained by measuring a total of 100 nanoparticles from five TEM images. UCNP-PVP features cubic structure with excellent crystallinity, as evinced by its typical selected area electron diffraction (SAED) pattern (Figure 1d) and X-ray power diffraction (XRD) spectrum as shown in Figure S1 in the Supporting Information. High-resolution TEM (HRTEM) measurement (Figure 1c) clearly demonstrates the presence of 2D lattice fringes, which are attributed to the (111) and (200) planes of a single UCNP-PVP nanoparticle, indexed from their corresponding Fourier transform (FT) diagram (Figure 1c, inset). The molar ratio of Na/Y/Yb/Er/F in UCNP-PVP was calculated to be 0.88:0.78:0.18:0.03:3.5 from the EDX spectrum (Figure S2). This agrees with the result of ICP-MS, which showed the ratio of Y/Yb/Er to be 0.81:0.17:0.016. Therefore, the molecular formula of UCNP-PVP can be approximately expressed as PVP/$NaYF_4$: 18% Yb, 2% Er. This lanthanide metal combination was chosen based on the literature[10,44] for the optimum upconversion luminescence. In this case, Er^{3+} ions would be surrounded by no Er^{3+} but several Yb^{3+} for facilitating excitation energy transfer. The Yb^{3+} ions can be separated by a sufficient number of optically inactive Y^{3+} ions to avoid energy migration to killer traps. Because branched PEI and PAA have abundant free amine and carboxylic acid groups and a higher binding affinity toward lanthanide ions than PVP, UCNP-PEI and UCNP-PAA can be readily produced by the replacement of PVP by PEI or PAA at 80 °C for 2 h. The resulting UCNP-PEI and UCNP-PAA maintained the same morphology and size distribution properties as UCNP-PVP (Figure 1e,f), indicating that these two coordinating polymers only interact with surface-exposed lanthanide ions to perform ligand exchange without destroying the inner structure of the whole particle. Meanwhile, three UCNPs have the same crystal structure (Figure S1), which can be indexed to the cubic phase of $NaYF_4$ with standard PDF card no. 77-2042. Due to the limitations of the TEM technique, a thin layer of organic coatings on the NP surface is hardly observed. Fortunately, Fourier transform infrared (FT-IR) spectra of polymer-coated UCNPs (Figure S3) clearly convey the presence of two absorption peaks at 2958 and 2847 cm^{-1}, which are the typical asymmetrical and symmetrical stretching vibrations of C—H in polymers and can be considered direct evidence of polymer coating. However, other IR absorption peaks are very difficult to assign because of the low sensitivity of the IR technique and severe interference from atmospheric water. It was reported by Li *et al.*[45,46] that bound oleic acid (OA) on the UCNPs' surface can be successfully detected by ^1H NMR analysis, where the capping ligands reached as much as 10 wt %. However, three polymer-coated UCNPs reported herein contain much fewer surface-coated molecules than that in OA-capped nanocrystals. Although ^1H NMR measurements were performed on the undoped $NaYF_4$ nanoparticles, we only got the ^1H NMR spectra with low signal-to-noise (S/N) ratio, failing to identify the nature of the trace amount of polymer coatings. Theoretically, the accurate amount of UCNP-linked PVP, PEI, and PAA molecules can be determined by thermogravimetric analysis (TGA), free amine quantification, and weak acid titration, respectively. By this means, the percentages of PVP that replaced by PEI or PAA can be known. However, there exists a huge error to measure PVP and PAA by TGA and titration. Fortunately, the PEI coating can be quantified by measuring the amount of reactive amine groups on UCNP-PEI. It was calculated to be 1.3 $\times 10^5$ NH_2 groups per particle by following reaction with *N*-succinimidyl 3-(2-pyridyldithio)propionate (SPDP) and measuring the absorbance of pyridine-2-thione at 343 nm.[47,48]

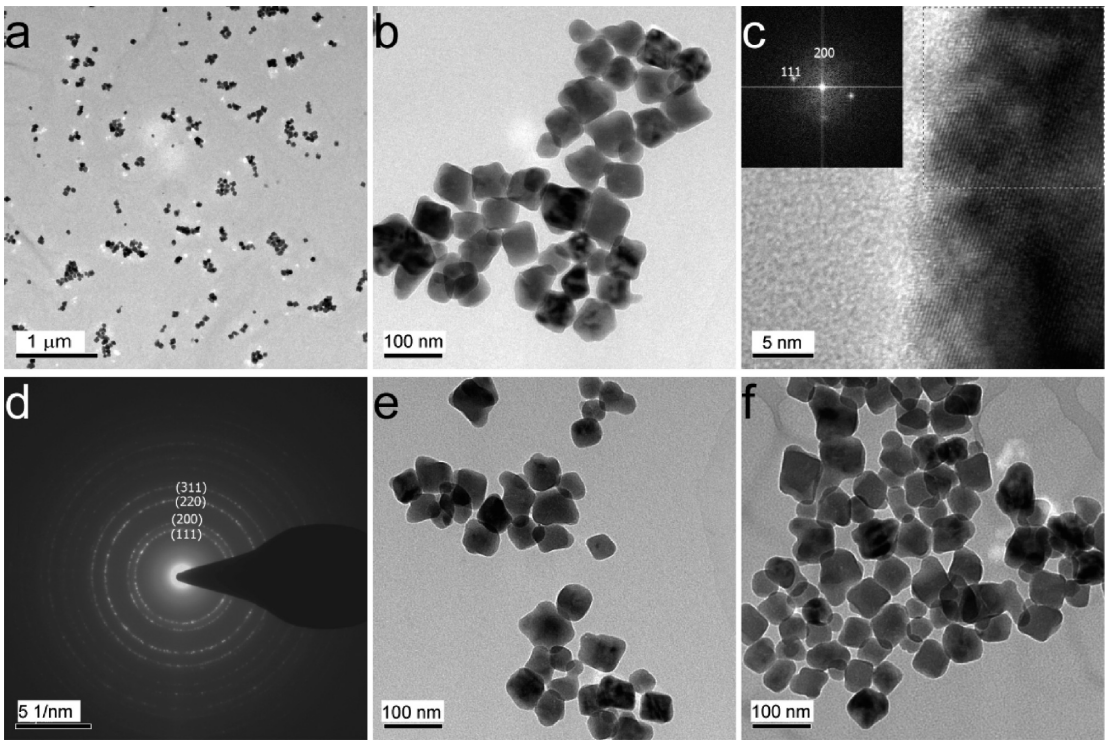

Figure 1. TEM characterization of $NaYF_4$:Yb/Er (18:2 mol %) nanoparticles with a series of polymer coatings. (a) Low-magnification, (b) high-magnification, (c) high-resolution TEM images of UCNP-PVP. Inset: Fourier transform diffractogram of selected dotted square shown in (c). (d) SAED pattern of UCNP-PVP. (e,f) TEM images of UCNP-PEI and UCNP-PAA, respectively. Scale bars are 1 μm for panel a, 100 nm for panels b, e, and f, and 5 nm for panel c.

Three polymer-coated UCNPs have a similar hydrodynamic diameter of about 150 nm, which was calculated from the cumulant analysis of the DLS results. Compared with TEM sizes, the significant increase of hydrodynamic diameters can be attributed to the dwelling effect of the outer layer of polymer coatings. Figure 2a shows the plot of the number percentage of UCNPs *versus* the logarithm of hydrodynamic size. UCNP-PAA demonstrates a slightly broader size distribution than that of UCNP-PEI and UCNP-PVP. Comparing PAA with PEI and PVP, a large number of carboxyl groups in PAA lead to strong hydrogen-bond interactions among PAA-coated UCNPs and thus make the UCNPs more agglomerative and polydisperse than UCNP-PEI and UCNP-PVP. Due to the modification of water-soluble and biocompatible polymers, UCNPs show excellent stability without any noticeable agglomeration in deionized water. Their long-term water stability (Figure S7) and nanoscale properties make them suitable for bioimaging applications. Although these polymer-coated UCNPs have similar TEM and DLS sizes, their ζ-potentials differ significantly (Figure 2b), 51.1, 10.2, and -22.6 mV for UCNP-PEI, UCNP-PVP, and UCNP-PAA, respectively. The slightly positive ζ-potential of UCNP-PVP might be a result from the protonation of the pyridinyl nitrogens on surface-bonded PVP moieties.[49,50] The dramatic difference of their ζ-potentials also indicates the successful conjugation of positively charged PEI and negatively charged PAA onto their corresponding UCNPs.

Photophysical Properties. These polymer-coated UCNPs, when excited under NIR light at 980 nm from an fiber-optic coupled diode laser, emit orange light that can be seen by naked eyes. This is due to the blending of its typical green luminescence with red luminescence. Figure 3 shows the upconversion luminescence spectra of UCNPs with a dispersion concentration of 1 mg/mL in water under 980 nm excitation at a power of 300 mV. Similar upconversion luminescence intensities were observed at the same dispersion concentration, indicating that three polymer coatings have similar influences on the luminescence efficiency of UCNPs. The upconversion luminescence can be split into two segments, a green region of 531−563 nm and a red region of 633−685 nm, which are ascribed to $^4S_{3/2}-{}^4I_{15/2}$ and $^4F_{9/2}-{}^4I_{15/2}$ transitions of doped Er^{3+} ions, respectively.[51]

Cytotoxicity Test. All of these polymer-coated UCNPs have potential as bioimaging nanoprobes due to their unique upconverting luminescence and good biocompatibility. However, cytotoxicity is a concern when it comes to the development of nanomaterials for biomedical imaging applications. The viability of HeLa and U87MG cells after exposure to UCNPs of different charges was measured by a standard MTT assay (Figure 4). UCNP-PAA showed negligible cytotoxicity toward both HeLa and U87MG cells, even at a high dosage of 0.5 mg/mL for 24 h. However, this was not the case for UCNP-PEI and UCNP-PVP. After treatment with 0.5 mg/mL of UCNP-PEI or UCNP-PVP for 24 h, the relative viability of HeLa and

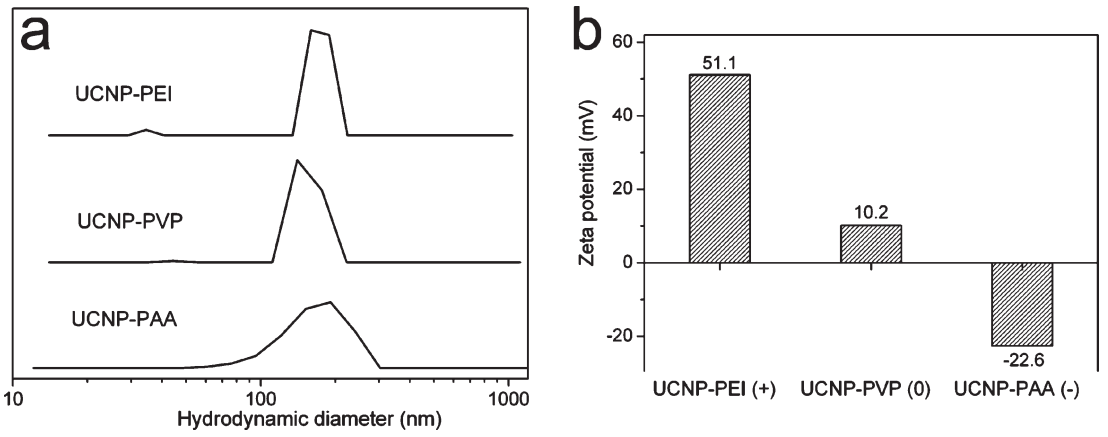

Figure 2. Percentage size distribution by number (a) and ζ-potential (b) of $NaYF_4:Yb^{3+}$, Er^{3+} NPs with various polymer coatings dispersed at the concentration of 1 mg/mL in deionized water.

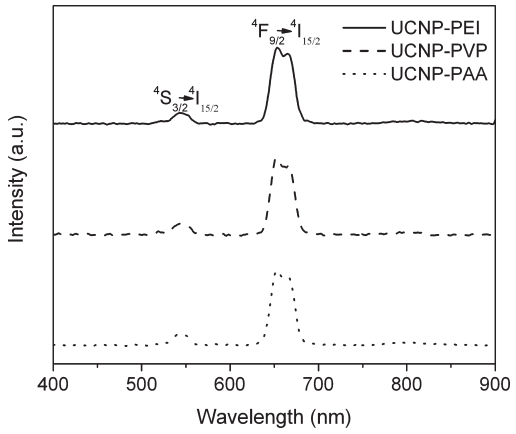

Figure 3. Upconversion luminescence spectra of polymer-coated UCNPs dispersed in water at the concentration of 1 mg/mL under excitation at 980 nm provided by fiber-optic coupled diode laser.

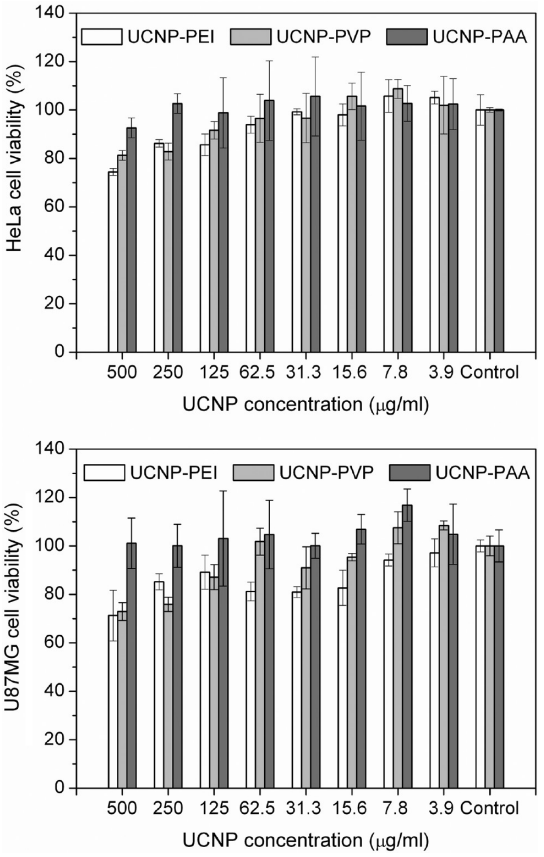

Figure 4. Relative cell viability of HeLa (top) and U87MG (bottom) cells after treating with different charged UCNPs of concentration ranging from 3.9 to 500 μg/mL for 24 h. Each data point was represented as mean ± SD from triplicate trials.

U87MG cells was reduced to 80% or even less. Since PEI has been reported to convey severe cytotoxicity,[52] it can be inferred that the moderate cytotoxicity of UCNP-PEI at high dosages originates from the surface PEI coating. Fortunately, cytotoxicity was not apparent after reducing UCNPs' concentration to 0.25 mg/mL, which is 5-fold higher than the concentration used in live-cell imaging. Taken together, it is evident that the cytotoxicity of UCNP-PEI and UCNP-PVP is tolerable, allowing for secure engineering of these UCNPs as live-cell imaging nanoprobes.

Surface-Charge-Dependent Cellular Uptake Studies. Cellular uptake behaviors of all UCNPs were visualized by multiphoton confocal live-cell imaging. Three carcinoma cell lines, HeLa cells (Figure 5), U87MG cells (Figure S4 in Supporting Information), and MCF-7 cells (Figure S5), were used. Cells stained by UCNPs were exposed to 980 nm irradiation using a femtosecond Ti:sapphire pulsed laser, and their typical upconversion luminescence was captured by photomultiplier tube (PMT) channels set at 540−560 and 640−660 nm for receiving green and red phosphorescent emissions, respectively. Since green and red emissions are closely and proportionally correlated, only green luminescence was selected for comparison, for simplicity's sake. For the positively charged UCNP-PEI, numerous bright green luminescent spots illuminating the cell cytoplasm were clearly observed in all cell lines studied. This spot-like emission pattern has been frequently observed in luminescent

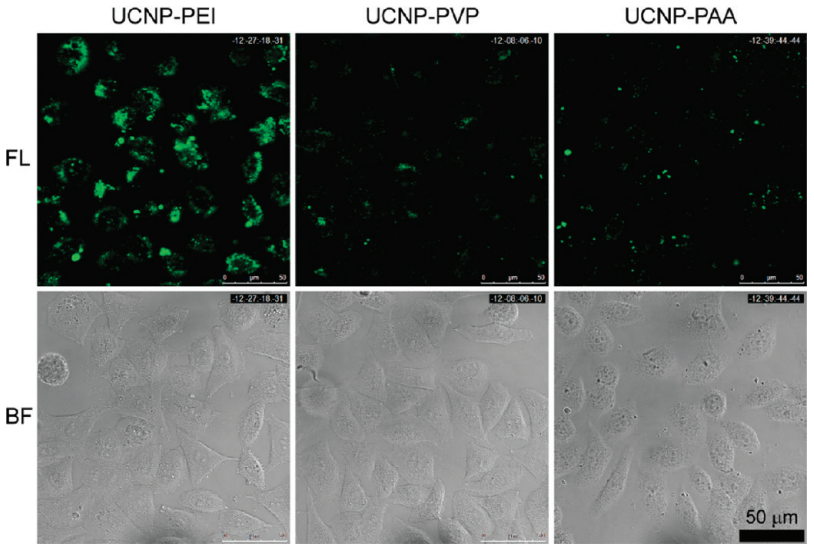

Figure 5. Multiphoton confocal fluorescent (top) and bright-field (bottom) images of HeLa cells following 24 h incubation with 50 μg/mL UCNP-PEI (left panel), UCNP-PVP (middle panel), and UCNP-PAA (right panel). The excitation at 980 nm was provided from a femtosecond Ti:sapphire pulsed laser, and the green emissions of 540−560 nm were acquired by a PMT channel (40× oil lens, scale bar = 50 μm).

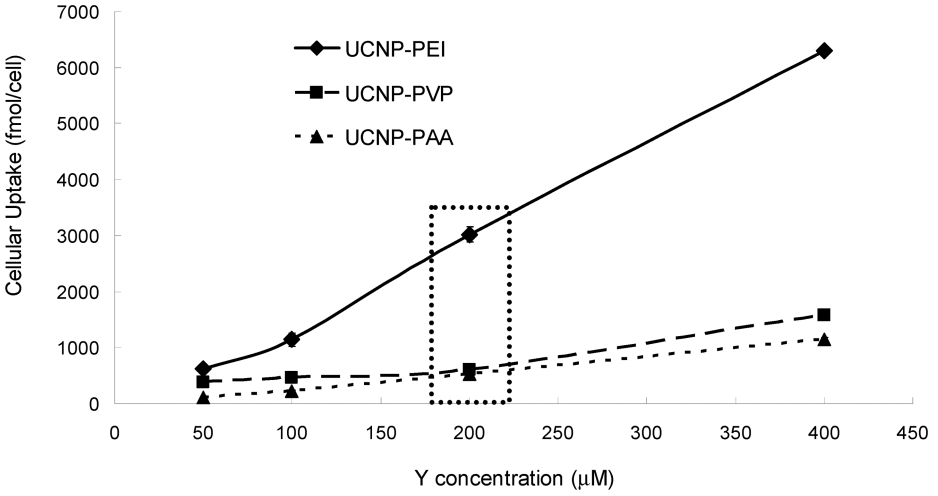

Figure 6. Average molar numbers of yttrium taken by a HeLa cell (fmol/cell) were determined by ICP-MS. HeLa cells were treated with polymer-coated UCNPs with yttrium concentration ranging from 50 to 400 μM at 37 °C for 24 h. Each data point was represented as mean ± SD from triplicate trials. Data points selected in the dotted rectangle box were acquired under the same conditions as used in multiphoton confocal imaging shown in Figure 5.

nanoparticles. On the contrary, UCNP-PVP and UCNP-PAA, under the same incubation and image acquisition conditions, demonstrated only a few illuminated spots with dim brightness. As shown in Figure 3, three UCNPs have similar upconverting efficiency in aqueous media, and thus it is reasonable to ascribe the brighter cell illumination of UCNP-PEI to its enhanced cellular uptake efficiency. To verify this hypothesis, ICP-MS was conducted to accurately quantify the trace amount of metal ions uptaken by cells. Y element, as the most abundant heavy metal in UCNPs, was chosen as a representative in order to measure the amount of uptaken nanoparticles. Upon 24 h incubation, all of the UCNPs show concentration-dependent cellular uptake in both HeLa (Figure 6) and U87MG (Figure S6) cell lines. In contrast to the relatively flat concentration-dependent cellular uptake profile of UCNP-PVP and UCNP-PAA, UCNP-PEI exhibits accelerating, concentration-dependent cellular uptake. When HeLa cells were treated with UCNPs of 200 μM Y for 24 h (dotted rectangle box in Figure 6), UCNP-PEI's cellular uptake is 5 times that of UCNP-PVP; UCNP-PAA shows the lowest cellular uptake efficiency. These are the same conditions used in multiphoton confocal cell imaging (Figure 5). On the basis of the consistent results of the cellular uptake investigations and the multiphoton confocal cell imaging, the order of uptake efficiency can be depicted as UCNP-PEI ≫ UCNP-PVP > UCNP-PAA. This distinct cellular uptake efficiency can be interpreted as the consequence of the electrostatic attraction of the negatively charged

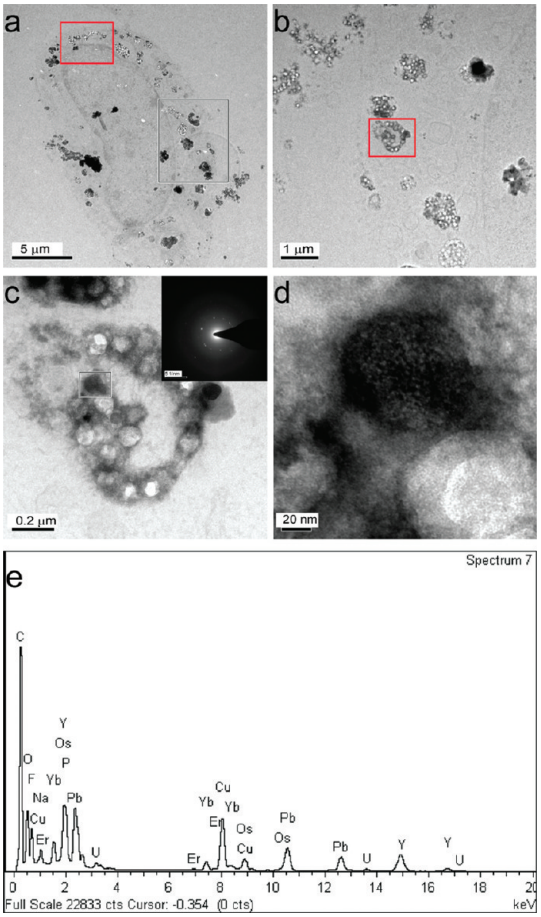

Figure 7. TEM images showing the compartmentalization of UCNP-PEI in HeLa cells (incubation with NPs at the concentration of 50 μg/mL at 37 °C for 24 h). Area of interest with red rectangle frame is magnified gradually from (a) to (d); inset of (c) is the SAED pattern of internalized UCNPs, and (e) is the EDX spectrum showing its corresponding elemental compositions to confirm the presence of UCNPs.

cell plasma membrane conferring a higher affinity to UCNP-PEI, as opposed to UCNP-PVP or UCNP-PAA.

Cellular Internalization Mechanism of UCNP-PEI. Resin section TEM is an important technique in biological electron microscopy; it provides direct evidence and clear, high-resolution pictures of NPs taken by cells and is extensively employed in cellular uptake mechanism studies. Since UCNP-PEI offers plenty of free amine groups, suitable for easy modification and can be effectively transported into cells, it is of importance to discover its cellular internalization mechanism. Upon incubation with 50 μg/mL of UCNP-PEI for 24 h, HeLa cells were fixed with cold methanol. The cells were detached by scraping, pelleted, and postfixed with osmium tetroxide and uranyl acetate. The fixed pellets were dehydrated with ethanol and further went through processes of resin infiltration, embedding, and cutting into 100 nm thick ultrathin sections with a glass/diamond knife for TEM study. All procedures were carried out according to the standard protocol for biological specimen preparation for TEM.[53] Figure 7a,b reveals that UCNP-PEI was trapped in vesicular structures decorated with some pits after being uptaken by HeLa cells, which can be seen clearly through enlarged images (Figure 7c, d). The chemical composition of uptaken UCNP-PEI remains unchanged, as shown by EDX spectrum (Figure 7e). The typical electron diffraction pattern of cubic structure $NaYF_4$ was also observed on the cells uptaken with UCNP-PEI (Figure 7c, inset), suggesting that the composition and nature of UCNP-PEI were retained after endocytosis. Careful observation on the high-magnification TEM image, shown in Figure 7d, leads to the postulation that the decorated pits adhering to UCNP-PEI may represent "protein-coated pits". These protein-coated pits are reported to be formed from assembly of high-affinity transmembrane receptors together with the bound ligands on the plasma membrane.[42] Thus this observation has pointed to the direction that the uptake mechanism of UCNP-PEI may go through protein-coated vesicular endocytosis. Two common protein coats that can be internalized are clathrin and caveolae. It should be noted that the following live-cell imaging studies (Figures 8 and 9) were performed on Zeiss Axiovert microscope without 980 nm excitation source. We thus partially labeled UCNP-PEI with fluorescein isothiocyanate (FITC),[11] and the green fluorescence from the surface-conjugated FITC, instead of the upconversion luminescence, was used to track the internalized UCNP-PEI. Because FITC labeling imposed minimal effects on the cellular internalization of the primary nanoparticles,[41] FITC-labeled UCNP-PEI quoted in Figures 8 and 9 was still denoted as UCNP-PEI. To visualize clathrin and caveolae, we constructed red fluorescent protein tagged clathrin (RFP-clathrin) and caveolae (RFP-caveolae) plasmids and independently expressed each plasmid into HeLa cells prior to UCNP-PEI (FITC-labeled) uptake. Time-lapse imaging studies reveal that UCNP-PEI did colocalize with RFP-clathrin at all time points (Figure 8) but not RFP-caveolae (data not shown). Clathrin vesicles are shown to move together with UCNP-PEI from the cell surface to the rim of the nuclear envelope. This observation suggests that UCNP-PEI entered HeLa cells mainly through clathrin-mediated endocytosis, and that the vesicles pictured in Figure 7a–d may represent clathrin, formed by invagination of the "coated pits".[42]

Effects of Chemical and Genetic Inhibitors on Endocytosis of UCNP-PEI. To further confirm that the route of UCNP-PEI uptake is through clathrin-mediated endocytosis, chemical inhibitors were employed to inhibit clathrin- or caveolae-mediated endocytosis.[54] Figure S8 (Supporting Information) shows that chlorpromazine inhibition of clathrin resulted in 31% decrease of internalization of UCNP-PEI revealed by ICP-MS measurement. In contrast, only 4% reduction of UCNP-PEI uptake could be detected when genistein was employed to suppress the function of caveolae. This set of data is indicative of clathrin receptors as the endocytic pathway of UCNP-PEI cellular uptake. However, due to the nonspecific nature of chemical inhibitors, the specific role that

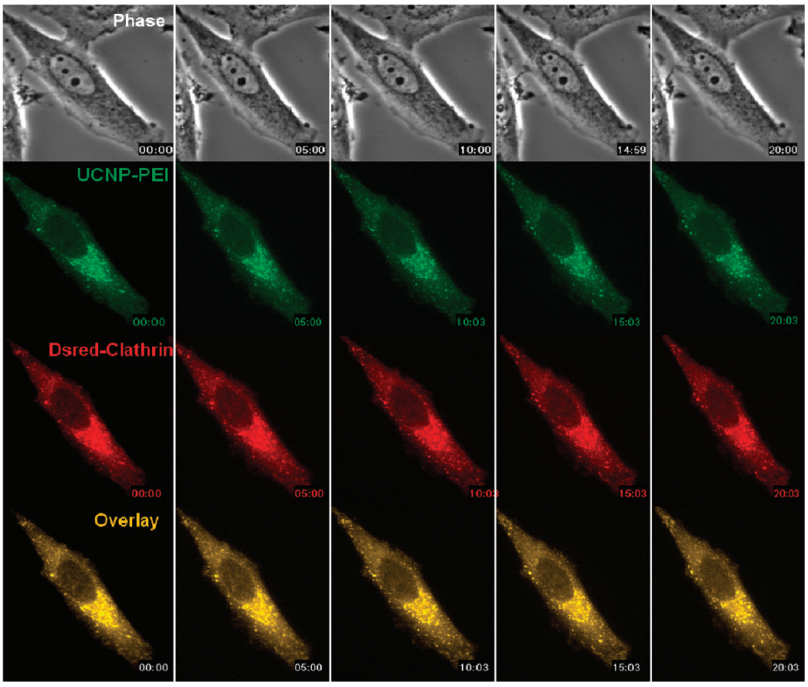

Figure 8. UCNP-PEI (FITC-labeled) uptake through clathrin-mediated endocytosis. HeLa cells transfected with RFP-tagged clathrin for 24 h. After transfection, UCNP-PEI was added subsequently to the culture, and live-cell imaging was started on the motorized stage of the Zeiss Axiovert microscope. Images were acquired at 5 min intervals with a Hamamatsu Orca camera for 16 h. MetaMorph imaging software was used as platforms for acquisition, assembly, analysis of colocalization, and deconvolution of the acquired time lapse images.

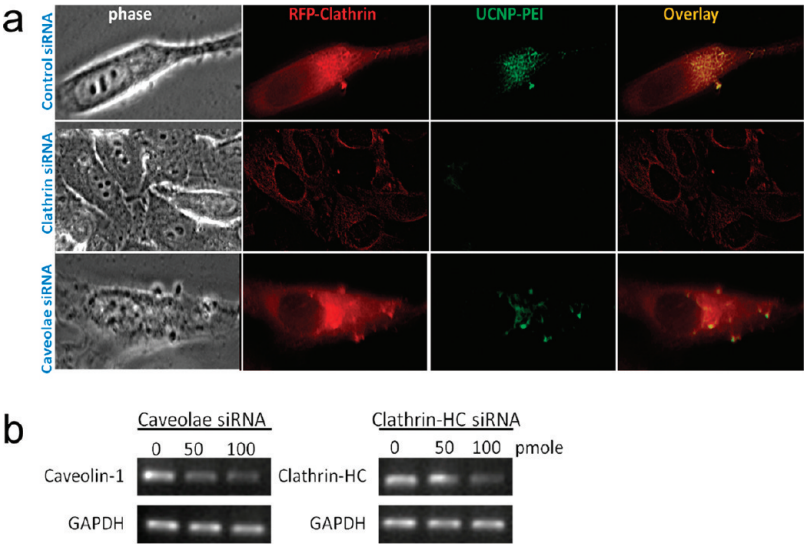

Figure 9. (a) Effects of genetic knockdown of clathrin receptors or caveolae receptors on UCNP-PEI (FITC-labeled) uptake. HeLa cells were cotransfected with RFP-clathrin together with either control scrambled siRNA, siRNA targeted against clathrin, or siRNA targeted against caveolin-1. The uptaking process of UCNP-PEI was monitored by live-cell imaging. (b) RT-PCR was performed to reveal the optimal siRNA amount to deplete more than 80% of the caveolae or the clathrin mRNA transcripts. GAPDH was used as a semiquantitative loading control.

chlorpromazine may play to achieve suppression of UCNP-PEI uptake is suboptimal (Figure S8). It is well-established that a knockdown approach using a genetic silencer is more specific yet less cytotoxic than chemical inhibitors, and thus we designed siRNAs to target against either the heavy chain of clathrin or caveolae. siRNA oligosequences were transfected into HeLa cells prior to UCNP-PEI (FITC-labeled) uptake. Successful knockdown of clathrin or caveolae was verified by reverse-transcription PCR (Figure 9b). By transfecting increasing amounts of siRNA against the specific targets, and after normalization with the loading control GAPDH, clathrin or caveolin mRNA transcripts were found to be reduced in a dose-dependent

manner (Figure 9b). An 80% in reduction in transcript levels could be detected by using 100 pmol of siRNA (Figure 9a, second row, and 9b). Indeed, live-cell imaging of UCNP-PEI reveals a complete retraction of UCNP-PEI uptake after genetic knockdown of clathrin as compared with HeLa cells transfected with control scrambled siRNA. Depletion of caveolin has minimal effect on the uptake of UCNP-PEI (Figure 9a, third row).

CONCLUSION

Three types of polymer-coated UCNPs were prepared through a hydrothermal reaction and then a ligand exchange process. They have similar TEM and DLS size, excellent water solubility, and similar upconverting luminescence efficiency, only differing in their ζ-potential values. However, their cellular uptake behaviors greatly vary, and therefore, it is concluded that the surface charge of UCNPs largely determines their cellular uptake efficiency. Positively charged UCNP-PEI has greatly enhanced cellular uptake, more than its neutral and negative counterparts, and it has the great potential to be applied in two-photon induced NIR live-cell imaging and further engineered as a specific intracellular nanoprobe. In addition, we have demonstrated that UCNP-PEI entered HeLa cells mainly through clarthin-mediated endocytosis. This study is the first report on the cellular uptake mechanism of positively charged UCNPs. Moreover, the ligand exchange approach provides us an effective tool to fine-tune the surface properties of NPs and further control their cell−nanoparticle interactions.

MATERIALS AND METHODS

Materials. Yttrium nitrate hexahydrate ($Y(NO_3)_3 \cdot 6H_2O$, 99.9%), sodium nitrate ($NaNO_3$, ≥99.0%), PVP (M_w ~55 kDa), PEI (branched, M_w ~25 kDa), PAA (M_w ~2000, 50 wt % in H_2O), and fluorescein isothiocyanate isomer I (FITC, ≥90%) were all purchased from Sigma-Aldrich. Ytterbium oxide (Yb_2O_3, 99.9%) and erbium oxide (Er_2O_3, 99.9%) were purchased from STREM. Ethylene glycol (EG, ≥99.0%) and ammonium fluoride (NH_4F, laboratory reagents) were purchased from Acros Organics and BDH Chemicals, respectively. All of the chemicals were used as received without further purification.

Synthesis. PVP-coated $NaYF_4$:18% Yb, 2% Er nanoparticles were prepared according to previously reported procedures[43] with slight modification. Yb_2O_3 (85.1 mg, 0.216 mmol) and Er_2O_3 (9.36 mg, 0.024 mmol) were dissolved in hot 10% HNO_3 and allowed to evaporate to dryness. Upon cooling, EG (80 mL) was poured in, followed by the subsequent addition of $Y(NO_3)_3 \cdot 6H_2O$ (0.7354 g, 1.92 mmol), PVP (2.2 g), and $NaNO_3$ (0.408 g, 4.8 mmol). The reaction mixture was heated to 80 °C for 10 min to a homogeneous solution with vigorous stirring, and then an EG (10 mL) solution of NH_4F (0.71 g, 19.2 mmol) was added dropwise. After aging at 80 °C for another 10 min, the reaction mixture was transferred to a 100 mL Teflon-lined stainless steel autoclave and was allowed to be treated hydrothermally at 180 °C for 3 h. After cooling to room temperature, the products were collected by centrifugation (10 min at 10 000 rpm), purified with distilled water and 95% ethanol three times, and dried in a vacuum oven at 80 °C overnight. Prepared white solid was denoted as UCNP-PVP. Ligand exchange treatment was carried out on UCNP-PVP according to the procedures reported by Li *et al.*[55] Briefly, for the synthesis of PEI-coated UNCPs, 50 mg of UCNP-PVP was dispersed in a 20 mL DMF solution containing 40 mg of branched PEI by sonication, and the reaction mixture was stirred at 80 °C for 2 h. After cooling, the products were isolated by centrifugation (20 min at 14 000 rpm), purified with distilled water and 95% ethanol three times, and completely dried in a vacuum oven at 80 °C overnight. The prepared light-green solid was denoted as UCNP-PEI. UCNP-PAA was prepared using the same procedures as UCNP-PEI, except using 80 mg of PAA (50 wt % in H_2O) instead of PEI, to perform ligand exchange reaction.

Characterization. TEM measurements were carried out on transmission electron microscope (Philips, Tecnai 20), equipped with an energy-dispersive X-ray spectrometer (EDX, Hitachi HF-2000). The operating voltage of the microscope was 200 kV. Upconversion fluorescent spectra were obtained on LS 55 fluorescence spectrophotometer (PerkinElmer Corp., Forster City, CA). An external 0−2 W adjustable diode laser integrated with an optical fiber (980 nm, Beijing Hi-Tech Optoelectronic Co., China) was used as the excitation source to replace the original xenon source in the spectrophotometer. DLS and ζ-potential measurements were performed on a Malvern Zetasizer 3000 HSA. XRD spectra were recorded on a Philips X'Pert MPD Pro X-ray diffractometer.

Cell Culture. Human cervical carcinoma HeLa cells (CCL-2, ATCC), human breast carcinoma MCF-7 cells (HTB-22, ATCC), and human glioblastoma U87MG cells (HTB-14, ATCC) were maintained in MEM (Eagle's minimum essential medium, Invitrogen), supplemented with 10% fetal bovine serum at 37 °C in a humidified atmosphere of 5% CO_2.

Cytotoxicity Assay. Cell viability was measured using a 3-(4,5-dimethylthiazol-2-yl)-2,5-diphenyltetrazolium bromide (MTT) proliferation assay. HeLa cells or U87MG cells were seeded in a 96-well flat-bottomed microplate (6000 cells/well) and cultured in 100 μL growth medium at 37 °C and 5% CO_2 for 24 h. Cell culture medium in each well was then replaced by 100 μL cell growth medium, containing UCNPs with concentrations ranging from 3.9 to 400 μg/mL. After incubation for 20 h, 20 μL of MTT (5 mg/mL in PBS solution) was added to each well, and cells were incubated further for 4 h at 37 °C. The growth medium was removed gently, and 200 μL of DMSO was then added to each well, sitting at room temperature overnight to dissolve the formazan crystals completely. The absorbance at the wavelength of 570 nm was measured by Multiskan EX (Thermo Electron Corporation), and each data point represents a mean ± SD from triplicate wells.

Cellular Uptake Measurement by ICP-MS. HeLa or U87MG cells were seeded onto 35 mm tissue culture dish (20 000 cells per dish) and incubated in 2 mL of culture medium at 37 °C for 24 h. The culture medium was replaced by the MEM solution containing polymer-coated UCNPs with yttrium concentration ranging from 50 to 400 μM (10−80 μg/mL of UCNPs). The cells were incubated in this culture medium at 37 °C for another 24 h. Cells in culture medium with no samples were used as controls. After rinsing with PBS three times, cells were trypsinized for cell counting, digested by 0.5 mL per dish of concentrated HNO_3 (≥69.5%, for trace analysis) at 70 °C for 3 h, and diluted by Milli-Q water to fill up to a 10 mL volumetric flask. Indium solution of 4 ppb was used as the internal standard. ICP-MS measurement was conducted on an Agilent 7500 series ICP-MS (Agilent Technologies), and every data point was expressed as a mean ± SD from triplicate dishes.

Live-Cell Multiphoton Confocal Microscopy Imaging. HeLa, U87MG, or MCF-7 cells were seeded on sterile glass coverslips in glass-bottomed 35 mm tissue culture dish. Fluorescence imaging was conducted on a Leica TCS SP5 equipped with a Ti:sapphire pulse laser. For live-cell imaging, the initial procedure was adopted from the ICP-MS one. After washing with PBS, cell-adhered

coverslips were mounted onto slides and immersed in CO_2-independent medium for imaging experiments.

Construction of Clathrin and Caveolin cDNA Plasmids. The cDNA encoding human caveolin-1 or clathrin heavy chain was subcloned into a red fluorescence protein vector backbone (Clontech), and the plasmids were transfected to HeLa cells by Fugene HD according to the manufacturer's protocol (Roche).

Gene Silencing Using siRNA and RT-PCR. For gene silencing studies, HeLa cells were transfected with 50−100 pmol of the specific siRNAs (clathrin HC, Invitrogen; caveolin, Santa Cruz). Cell extracts were harvested 48 h after transfection for total RNA isolation using Trizol reagent (Invitrogen), and 5 μg of the total RNA was reverse transcribed with an oligo-dT primer and Superscript II reverse transcriptase (Invitrogen). One-tenth of the first strand cDNA was used for semiquantitative measurements (normalized by the GAPDH transcript level) of clathrin, caveolae transcript levels with specific primers:

Clathrin HC-Forward	GGCCCAGATTCTGCCAATTCGTTT
Clathrin HC-Reverse	TGATGGCGCTGTCTGCTGAAATTG
Caveolin-1-Forward	ACCTCAACGATGACGTGGTCAAGA
Caveolin-1-Reverse	TGGAATAGACACGGCTGATGCACT

The PCR products were electrophoresed in 1% agarose gels and stained by ethidium bromide. The optimal dosage of siRNA was then used to perform live-cell imaging to determine the UCNP-PEI uptake pathway.

Cellular Internalization Pathways Revealed by Colocalization and Genetic Inhibition. For the clathrin-mediated endocytosis studies, HeLa cells were seeded onto MatTek dishes and transfected with RFP-tagged clathrin or co-transfected with RFP-tagged clathrin plus specific siRNA sequences targeting against clathrin heavy chain or caveolin-1 or scrambled siRNA, using HD Fugene, for 24 h. After transfection, UCNP-PEI (FITC-labeled) was added subsequently to the culture, and live-cell imaging was conducted on the motorized stage of the Zeiss Axiovert microscope. Images were acquired at 5 min intervals with Hamamatsu Orca camera (Hamamatsu Photonics) for 16 h. MetaMorph imaging software (Molecular Device) was used as the platform for acquisition, assembly, analysis of co-localization, and deconvolution of the time-lapse images.

Cellular Internalization Pathways Revealed by Chemical Inhibition. Chlorpromazine (10 μg/mL) and genistein (200 μM) were chosen as chemical inhibitors to suppress clathrin- and caveolae-mediated endocytosis, respectively.[54] HeLa cells were seeded onto 35 mm tissue culture dish (20 000 cells per dish) and incubated with inhibitors in serum-free MEM for 1 h before incubation with 40 μg/mL UCNPs (200 μM Y) plus inhibitors in fresh MEM for 1 h. HeLa cells treated with UCNPs in the absence of inhibitors were taken as controls. The cellular uptake amount was measured by ICP-MS.

Acknowledgment. This work was funded by grants from The Hong Kong Research Grants Council (PolyU 503510P), The University of Hong Kong and Shenzhen Bioindustry Development Fund-Basic Research Program (JC201005280607A). We acknowledge City University of Hong Kong for providing laser scanning confocal microscope facilities. J.J. acknowledges the receipt of postgraduate studentship administrated by The University of Hong Kong. J.J. also thanks Prof. Marie C. Lin for technical assistance and helpful discussions.

Supporting Information Available: XRD patterns, EDX, FT-IR spectra, and long-term stability test of polymer-coated UCNPs; multiphoton confocal imaging micrographs of U87MG and MCF-7 cells stained by polymer-coated UCNPs; cellular uptake of UCNPs in U87MG cells; chemical inhibitor studies. This material is available free of charge *via* the Internet at http://pubs.acs.org.

REFERENCES AND NOTES

1. Stephens, D. J.; Allan, V. J. Light Microscopy Techniques for Live Cell Imaging. *Science* **2003**, *300*, 82–86.
2. Wang, Y.; Shyy, J. Y. J.; Chien, S. Fluorescence Proteins, Live-Cell Imaging, and Mechanobiology: Seeing Is Believing. *Annu. Rev. Biomed. Eng.* **2008**, *10*, 1–38.
3. Frangioni, J. V. *In Vivo* Near-Infrared Fluorescence Imaging. *Curr. Opin. Chem. Biol.* **2003**, *7*, 626–634.
4. Hilderbrand, S. A.; Weissleder, R. Near-Infrared Fluorescence: Application to *In Vivo* Molecular Imaging. *Curr. Opin. Chem. Biol.* **2010**, *14*, 71–79.
5. Gao, J.; Chen, X.; Cheng, Z. Near-Infrared Quantum Dots as Optical Probes for Tumor Imaging. *Curr. Top. Med. Chem.* **2010**, *10*, 1147–1157.
6. Weber, J. Continuously UV-Bleaching of Organic Laser Dyes. *Phys. Lett. A* **1973**, *45*, 35–36.
7. Hardman, R. A Toxicologic Review of Quantum Dots: Toxicity Depends on Physicochemical and Environmental Factors. *Environ. Health Perspect.* **2006**, *114*, 165–172.
8. Shen, J.; Sun, L. D.; Yan, C. H. Luminescent Rare Earth Nanomaterials for Bioprobe Applications. *Dalton Trans.* **2008**, 5687–5697.
9. Wang, F.; Liu, X. Recent Advances in the Chemistry of Lanthanide-Doped Upconversion Nanocrystals. *Chem. Soc. Rev.* **2009**, *38*, 976–989.
10. Auzel, F. Upconversion and Anti-Stokes Processes with f and d Ions in Solids. *Chem. Rev.* **2004**, *104*, 139–174.
11. Wang, F.; Liu, X. Upconversion Multicolor Fine-Tuning: Visible to Near-Infrared Emission from Lanthanide-Doped $NaYF_4$ Nanoparticles. *J. Am. Chem. Soc.* **2008**, *130*, 5642–5643.
12. van de Rijke, F.; Zijlmans, H.; Li, S.; Vail, T.; Raap, A. K.; Niedbala, R. S.; Tanke, H. J. Up-Converting Phosphor Reporters for Nucleic Acid Microarrays. *Nat. Biotechnol.* **2001**, *19*, 273–276.
13. Wang, L.; Li, Y. Green Upconversion Nanocrystals for DNA Detection. *Chem. Commun.* **2006**, 2557–2559.
14. Zhang, P.; Rogelj, S.; Nguyen, K.; Wheeler, D. Design of a Highly Sensitive and Specific Nucleotide Sensor Based on Photon Upconverting Particles. *J. Am. Chem. Soc.* **2006**, *128*, 12410–12411.
15. Kumar, M.; Zhang, P. Highly Sensitive and Selective Label-Free Optical Detection of DNA Hybridization Based on Photon Upconverting Nanoparticles. *Langmuir* **2009**, *25*, 6024–6027.
16. Shan, J.; Chen, J.; Meng, J.; Collins, J.; Soboyejo, W.; Friedberg, J. S.; Ju, Y. Biofunctionalization, Cytotoxicity, and Cell Uptake of Lanthanide Doped Hydrophobically Ligated $NaYF_4$ Upconversion Nanophosphors. *J. Appl. Phys.* **2008**, *104*, 094308.
17. Park, Y. I.; Kim, J. H.; Lee, K. T.; Jeon, K. S.; Na, H. B.; Yu, J. H.; Kim, H. M.; Lee, N.; Choi, S. H.; Baik, S. I. Nonblinking and Nonbleaching Upconverting Nanoparticles as an Optical Imaging Nanoprobe and T_1 Magnetic Resonance Imaging Contrast Agent. *Adv. Mater.* **2009**, *21*, 4467–4471.
18. Traina, C. A.; Dennes, T. J.; Schwartz, J. A Modular Monolayer Coating Enables Cell Targeting by Luminescent Yttria Nanoparticles. *Bioconjugate Chem.* **2009**, *20*, 437–439.
19. Wang, M.; Mi, C. C.; Wang, W. X.; Liu, C. H.; Wu, Y. F.; Xu, Z. R.; Mao, C. B.; Xu, S. K. Immunolabeling and NIR-Excited Fluorescent Imaging of HeLa Cells by Using $NaYF_4$: Yb, Er Upconversion Nanoparticles. *ACS Nano* **2009**, *3*, 1580–1586.
20. Zako, T.; Nagata, H.; Terada, N.; Utsumi, A.; Sakono, M.; Yohda, M.; Ueda, H.; Soga, K.; Maeda, M. Cyclic RGD Peptide-Labeled Upconversion Nanophosphors for Tumor Cell-Targeted Imaging. *Biochem. Biophys. Res. Commun.* **2009**, *381*, 54–58.
21. Chen, Q.; Wang, X.; Chen, F.; Zhang, Q.; Dong, B.; Yang, H.; Liu, G.; Zhu, Y. Functionalization of Upconverted Luminescent $NaYF_4$: Yb/Er Nanocrystals by Folic Acid−Chitosan Conjugates for Targeted Lung Cancer Cell Imaging. *J. Mater. Chem.* **2011**, *21*, 7661–7667.
22. Yu, M.; Li, F.; Chen, Z.; Hu, H.; Zhan, C.; Yang, H.; Huang, C. Laser Scanning Up-Conversion Luminescence Microscopy for Imaging Cells Labeled with Rare-Earth Nanophosphors. *Anal. Chem.* **2009**, *81*, 930–935.
23. Lim, S. F.; Riehn, R.; Ryu, W. S.; Khanarian, N.; Tung, C.; Tank, D.; Austin, R. H. *In Vivo* and Scanning Electron Microscopy Imaging of Upconverting Nanophosphors in *Caenorhabditis elegans*. *Nano Lett.* **2006**, *6*, 169–174.

24. Chatterjee, D. K.; Rufaihah, A. J.; Zhang, Y. Upconversion Fluorescence Imaging of Cells and Small Animals Using Lanthanide Doped Nanocrystals. *Biomaterials* **2008**, *29*, 937–943.
25. Nyk, M.; Kumar, R.; Ohulchanskyy, T. Y.; Bergey, E. J.; Prasad, P. N. High Contrast *In Vitro* and *In Vivo* Photoluminescence Bioimaging Using Near Infrared to Near Infrared Up-Conversion in Tm^{3+} and Yb^{3+} Doped Fluoride Nanophosphors. *Nano Lett.* **2008**, *8*, 3834–3838.
26. Hilderbrand, S. A.; Shao, F.; Salthouse, C.; Mahmood, U.; Weissleder, R. Upconverting Luminescent Nanomaterials: Application to *In Vivo* Bioimaging. *Chem. Commun.* **2009**, 4188–4190.
27. Idris, N. M.; Li, Z.; Ye, L.; Wei Sim, E. K.; Mahendran, R.; Ho, P. C. L.; Zhang, Y. Tracking Transplanted Cells in Live Animal Using Upconversion Fluorescent Nanoparticles. *Biomaterials* **2009**, *30*, 5104–5113.
28. Xiong, L. Q.; Chen, Z. G.; Yu, M. X.; Li, F. Y.; Liu, C.; Huang, C. H. Synthesis, Characterization, and *In Vivo* Targeted Imaging of Amine-Functionalized Rare-Earth Up-Converting Nanophosphors. *Biomaterials* **2009**, *30*, 5592–5600.
29. Yu, X.-F.; Sun, Z.; Li, M.; Xiang, Y.; Wang, Q.-Q.; Tang, F.; Wu, Y.; Cao, Z.; Li, W. Neurotoxin-Conjugated Upconversion Nanoprobes for Direct Visualization of Tumors under Near-Infrared Irradiation. *Biomaterials* **2010**, *31*, 8724–8731.
30. Zhou, J.; Yu, M.; Sun, Y.; Zhang, X.; Zhu, X.; Wu, Z.; Wu, D.; Li, F. Fluorine-18-Labeled $Gd^{3+}/Yb^{3+}/Er^{3+}$ Co-Doped $NaYF_4$ Nanophosphors for Multimodality PET/MR/UCL Imaging. *Biomaterials* **2010**, *32*, 1148–1156.
31. Cao, T.; Yang, Y.; Gao, Y.; Zhou, J.; Li, Z.; Li, F. High-Quality Water-Soluble and Surface-Functionalized Upconversion Nanocrystals as Luminescent Probes for Bioimaging. *Biomaterials* **2011**, *32*, 2959–2968.
32. Liu, Q.; Sun, Y.; Li, C.; Zhou, J.; Li, C.; Yang, T.; Zhang, X.; Yi, T.; Wu, D.; Li, F. ^{18}F-Labeled Magnetic-Upconversion Nanophosphors *via* Rare-Earth Cation-Assisted Ligand Assembly. *ACS Nano* **2011**, *5*, 3146–3157.
33. Sun, Y.; Yu, M.; Liang, S.; Zhang, Y.; Li, C.; Mou, T.; Yang, W.; Zhang, X.; Li, B.; Huang, C.; Li, F. Fluorine-18 Labeled Rare-Earth Nanoparticles for Positron Emission Tomography (PET) Imaging of Sentinel Lymph Node. *Biomaterials* **2011**, *32*, 2999–3007.
34. Wang, Z.-L.; Hao, J.; Chan, H. L. W.; Law, G.-L.; Wong, W.-T.; Wong, K.-L.; Murphy, M. B.; Su, T.; Zhang, Z. H.; Zeng, S. Q. Simultaneous Synthesis and Functionalization of Water-Soluble Up-Conversion Nanoparticles for *In-Vitro* Cell and Nude Mouse Imaging. *Nanoscale* **2011**, *3*, 2175–2181.
35. Zhan, Q.; Qian, J.; Liang, H.; Somesfalean, G.; Wang, D.; He, S.; Zhang, Z.; Andersson-Engels, S. Using 915 nm Laser Excited $Tm^{3+}/Er^{3+}/Ho^{3+}$-Doped $NaYbF_4$ Upconversion Nanoparticles for *In Vitro* and Deeper *In Vivo* Bioimaging without Overheating Irradiation. *ACS Nano* **2011**, *5*, 3744–3757.
36. Jiang, S.; Zhang, Y.; Lim, K. M.; Sim, E. K. W.; Ye, L. NIR-to-Visible Upconversion Nanoparticles for Fluorescent Labeling and Targeted Delivery of siRNA. *Nanotechnology* **2009**, *20*, 155101.
37. Wang, C.; Cheng, L.; Liu, Z. Drug Delivery with Upconversion Nanoparticles for Multi-functional Targeted Cancer Cell Imaging and Therapy. *Biomaterials* **2010**, *32*, 1110–1120.
38. Guo, H.; Qian, H.; Idris, N. M.; Zhang, Y. Singlet Oxygen-Induced Apoptosis of Cancer Cells Using Upconversion Fluorescent Nanoparticles as a Carrier of Photosensitizer. *Nanomedicine* **2010**, *6*, 486–495.
39. Verma, A.; Stellacci, F. Effect of Surface Properties on Nanoparticle−Cell Interactions. *Small* **2010**, *6*, 12–21.
40. Arvizo, R. R.; Miranda, O. R.; Thompson, M. A.; Pabelick, C. M.; Bhattacharya, R.; Robertson, J. D.; Rotello, V. M.; Prakash, Y. S.; Mukherjee, P. Effect of Nanoparticle Surface Charge at the Plasma Membrane and Beyond. *Nano Lett.* **2010**, *10*, 2543–2548.
41. Asati, A.; Santra, S.; Kaittanis, C.; Perez, J. M. Surface-Charge-Dependent Cell Localization and Cytotoxicity of Cerium Oxide Nanoparticles. *ACS Nano* **2010**, *4*, 5321–5331.
42. Conner, S. D.; Schmid, S. L. Regulated Portals of Entry into the Cell. *Nature* **2003**, *422*, 37–44.
43. Li, Z. Q.; Zhang, Y. Monodisperse Silica-Coated Polyvinylpyrrolidone/$NaYF_4$ Nanocrystals with Multicolor Upconversion Fluorescence Emission. *Angew. Chem., Int. Ed.* **2006**, *45*, 7732–7735.
44. Krmer, K. W.; Biner, D.; Frei, G.; Güdel, H. U.; Hehlen, M. P.; Luethi, S. R. Hexagonal Sodium Yttrium Fluoride Based Green and Blue Emitting Upconversion Phosphors. *Chem. Mater.* **2004**, *16*, 1244–1251.
45. Hu, H.; Yu, M.; Li, F.; Chen, Z.; Gao, X.; Xiong, L.; Huang, C. Facile Epoxidation Strategy for Producing Amphiphilic Up-Converting Rare-Earth Nanophosphors as Biological Labels. *Chem. Mater.* **2008**, *20*, 7003–7009.
46. Chen, Z.; Chen, H.; Hu, H.; Yu, M.; Li, F.; Zhang, Q.; Zhou, Z.; Yi, T.; Huang, C. Versatile Synthesis Strategy for Carboxylic Acid-Functionalized Upconverting Nanophosphors as Biological Labels. *J. Am. Chem. Soc.* **2008**, *130*, 3023–3029.
47. Fang, C.; Bhattarai, N.; Sun, C.; Zhang, M. Functionalized Nanoparticles with Long-Term Stability in Biological Media *Small* **2009**, *5*, 1637–1641.
48. Schellenberger, E. A.; Sosnovik, D.; Weissleder, R.; Josephson, L. Magneto/Optical Annexin V, a Multimodal Protein. *Bioconjugate Chem.* **2004**, *15*, 1062–1067.
49. Li, D.; He, Q.; Yang, Y.; Mohwald, H.; Li, J. Two-Stage pH Response of Poly(4-vinylpyridine) Grafted Gold Nanoparticles. *Macromolecules* **2008**, *41*, 7254–7256.
50. Urch, H.; Vallet-Regi, M.; Ruiz, L.; Gonzalez-Calbet, J.; Epple, M. Calcium Phosphate Nanoparticles with Adjustable Dispersability and Crystallinity. *J. Mater. Chem.* **2009**, *19*, 2166–2171.
51. Wang, F.; Chatterjee, D. K.; Li, Z. Q.; Zhang, Y.; Fan, X. P.; Wang, M. Q. Synthesis of Polyethylenimine/$NaYF_4$ Nanoparticles with Upconversion Fluorescence. *Nanotechnology* **2006**, *17*, 5786–5791.
52. Boussif, O.; Lezoualc'h, F.; Zanta, M. A.; Mergny, M. D.; Scherman, D.; Demeneix, B.; Behr, J. P. A Versatile Vector for Gene and Oligonucleotide Transfer into Cells in Culture and *in Vivo*: Polyethylenimine. *Proc. Natl. Acad. Sci. U.S.A.* **1995**, *92*, 7297–7301.
53. Glauert, A. M.; Lewis, P. R. *Biological Specimen Preparation for Transmission Electron Microscopy*; Princeton University Press: Princeton, NJ, 1998.
54. Gratton, S. E. A.; Ropp, P. A.; Pohlhaus, P. D.; Luft, J. C.; Madden, V. J.; Napier, M. E.; DeSimone, J. M. The Effect of Particle Design on Cellular Internalization Pathways. *Proc. Natl. Acad. Sci. U.S.A.* **2008**, *105*, 11613–11618.
55. Xiong, L.; Yang, T.; Yang, Y.; Xu, C.; Li, F. Long-Term *In Vivo* Biodistribution Imaging and Toxicity of Polyacrylic Acid-Coated Upconversion Nanophosphors. *Biomaterials* **2010**, *31*, 7078–7085.